Geophysical Research Letters®

RESEARCH LETTER
10.1029/2021GL093803

Key Points:

- Climate projections for the tropical Atlantic sector depend on the quality of simulating present-day conditions
- Less biased climate models provide more reliable projections
- Spread in CO_2-forced climate changes over the Tropical Atlantic region

Supporting Information:

Supporting Information may be found in the online version of this article.

Correspondence to:

M. Latif,
mlatif@geomar.de

Citation:

Imbol Nkwinkwa, A. S. N., Latif, M., & Park, W. (2021). Mean-state dependence of CO_2-forced tropical Atlantic sector climate change. *Geophysical Research Letters*, *48*, e2021GL093803. https://doi.org/10.1029/2021GL093803

Received 28 APR 2021
Accepted 30 AUG 2021

Author Contributions:

Conceptualization: M. Latif, W. Park
Data curation: A. S. N. Imbol Nkwinkwa
Formal analysis: A. S. N. Imbol Nkwinkwa
Funding acquisition: M. Latif
Writing – original draft: M. Latif
Writing – review & editing: A. S. N. Imbol Nkwinkwa, M. Latif, W. Park

Mean-State Dependence of CO_2-Forced Tropical Atlantic Sector Climate Change

A. S. N. Imbol Nkwinkwa[1], M. Latif[1,2], and W. Park[1]

[1]GEOMAR Helmholtz Centre for Ocean Research Kiel, Kiel, Germany, [2]Faculty of Mathematics and Natural Sciences, University of Kiel, Kiel, Germany

Abstract Twenty-first-century climate change projections are uncertain, especially on regional scales. An important source of uncertainty is that climate models exhibit biases, which limits their ability to predict climate. One of the largest biases is the too warm sea surface temperature (SST) in the eastern tropical Atlantic (TA), reflecting deficient atmospheric and oceanic circulation. Here, we show that CO_2-forced TA-sector climate changes simulated by state-of-the-art climate models exhibit a strong mean-state dependence. In particular, models simulating largest SST warming in the eastern TA, consistent with the warming observed since the mid-20th century, typically exhibit a more realistic mean state than models simulating largest warming in the western TA. The former models exhibit a larger climate sensitivity, and predict stronger and in part qualitatively different climate changes over the TA sector, for example in precipitation. These findings may help to reducing uncertainty in TA-climate change projections.

Plain Language Summary Twenty-first-century climate change projections are uncertain, especially on regional scales. An important source of uncertainty is that climate models exhibit biases, which limits their ability to predict climate. One of the largest biases is the too warm sea surface temperature in the eastern tropical Atlantic (TA), reflecting deficient atmospheric and oceanic circulation. Here, we show that CO_2-forced TA-sector climate changes simulated by state-of-the-art climate models exhibit a strong relationship to the quality of simulating the mean state. These findings may help to reducing uncertainty in climate change projections over the TA sector.

1. Introduction

The Earth's surface has warmed in the global average by just more than 1°C relative to preindustrial times, largely in response to rising carbon dioxide (CO_2) concentrations due to anthropogenic emissions (IPCC, 2014). Since the beginning of the industrialization, the atmospheric CO_2-concentration has increased by almost 50% and the current concentration could be unprecedented during the last 3 million years (Willeit et al., 2019). Climate models project a global surface warming during the 21st century of a scale, with regard to speed and magnitude, that mankind has not experienced to date should the atmospheric CO_2-concentrations continue to rise unabatedly (IPCC, 2014).

Uncertainty in the projected climate changes, however, is large due to internal variability (Deser et al., 2020; Kay et al., 2015; Wills et al., 2020), scenario and model uncertainty (Hawkins & Sutton, 2009; Shepherd, 2014), where, the latter also is termed response uncertainty. Here, we are concerned with the latter source of uncertainty, specifically the relation of CO_2-forced climate changes over the TA to the models' mean state. A long-standing problem in many climate models is the warm sea surface temperature (SST) bias in the eastern tropical Atlantic (TA) (warm bias hereafter; Davey et al., 2002; Richter & Xie, 2008; Richter et al., 2014; Steinig et al., 2018), which is due to the models' inability to realistically simulate the so-called cold tongue, a large pool of locally colder ocean surface water that develops each boreal spring, is centered just south of the equator and lasts through boreal summer. The warm bias is an expression of biases in oceanic (Cabos et al., 2017; Richter & Tokinaga, 2020; Xu et al., 2014) and atmospheric circulations (Harlaβ et al., 2018; Meynadier et al., 2016; Milinski et al., 2016; Siongco et al., 2015; Zuidema et al., 2016), and it goes along with erroneous precipitation patterns (Richter & Xie, 2008; Steinig et al., 2018). This study investigates the large spread in CO_2-forced climate changes over the TA region that is observed even when identical greenhouse gas forcing is applied to the models.

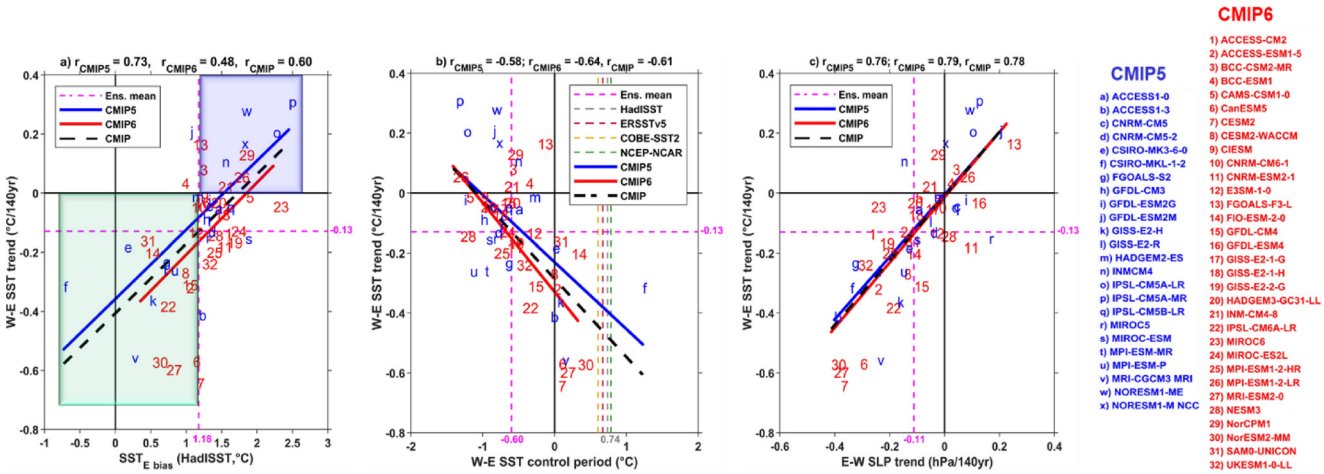

Figure 1. Relation of CO_2-forced sea surface temperature (SST) gradient change to SST bias, mean-state SST gradient and CO_2-forced sea level pressure (SLP) gradient change. (a) SST bias (°C) in the eastern equatorial Atlantic (green box in Figure 2a and 2b) in the CMIP5 (blue letters) and CMIP6 models (red numbers) and its relationship to the CO_2-forced trend in the SST gradient (°C/140 years) across the equatorial Atlantic. The vertical purple dashed line denotes the ensemble-mean SST bias, the horizontal purple dashed line the ensemble-mean trend in the SST gradient (°C/140 years). A positive (negative) change in the SST gradient indicates strengthening (weakening) zonal SST contrast. Green (blue) shaded areas denote the space of the ETA (WTA) models. (b) Simulated zonal SST gradient (°C) during the first 30 years (F30) versus the CO_2-forced trends in zonal SST gradient (°C/140 years). Vertical green, gray, red and orange dashed lines indicate observations. (c) CO_2-forced trends in zonal SST gradient (°C/140 years) versus CO_2-forced trends in zonal SLP gradient (hPa/140 years). Zonal gradients are calculated using the boxes shown in Figures 2a and 2b and defined as the difference between the western and the eastern box (W–E) for SST and the difference between the eastern and the western box (E–W) for SLP. The correlations in (a), (b), and (c) are statistically significant at the 95% level according to a Student's t-test. Regression lines in (a), (b), and (c) are given for all Coupled Model Intercomparison Project (CMIP) models (black dashed), CMIP5 models (blue), and CMIP6 models (red).

2. Data

We investigate 56 global warming simulations with models participating in the two latest phases of the Coupled Model Intercomparison Project (CMIP), CMIP5 (24 models, Table S1, Taylor et al., 2012) and CMIP6 (32 models, Table S2, Eyring et al., 2016). Only one realization has been used from each model. In the simulations, termed 1pctCO_2, atmospheric CO_2-levels rise at a rate of 1% per year (compound), starting from preindustrial levels and doubling (quadrupling) after 70 (140) years. A comparison between the CMIP5 and CMIP6 models is found in Richter and Tokinaga (2020). Here, the CMIP5 and CMIP6 models are treated as one ensemble to increase ensemble size, as, with the exception of SST and precipitation, not all variables considered in this study are available from every model (Table S3). All climate models belonging to the same family have been retained in the analyses, because models of the same family can considerably differ when only varying a few parameters, for example two parameters in the atmospheric convection scheme of the Kiel Climate Model (KCM, Wengel et al., 2018). We note that when removing "redundant" models, the results basically remain unchanged, which, however, only was tested with the CMIP6 models. The CO_2-forced response is shown by linear trends calculated over all 140 years and all seasons. Ensemble-mean spatial patterns computed from all models and seasonal results are shown in the Figures S1–S3. For reference, SST and sea level pressure (SLP) data from different sources is used (Supporting Information S1). Reanalysis data are from ECMWF ERA-5 (Hersbach et al., 2019).

3. CO_2-Forced Climate Changes

3.1. Box-Based Indices

An index of the warm bias is defined as the departure of the simulated SST, averaged over the eastern equatorial Atlantic (4.5°N–4.5°S, 10°E–20°W; green box in Figures 2a and 2b) and the first 30 years (F30 hereafter), from the observed SST averaged over 1950–2019. The overwhelming majority of the models exhibit a relatively large warm bias (Figure 1a). Only one model belonging to the CMIP5 ensemble exhibits a cold bias. The ensemble-mean warm bias is 1.18°C with a range of 3.3°C (−0.8°C–+2.5°C). An index of the SST contrast across the equatorial Atlantic (SST gradient hereafter) is defined as the difference between the

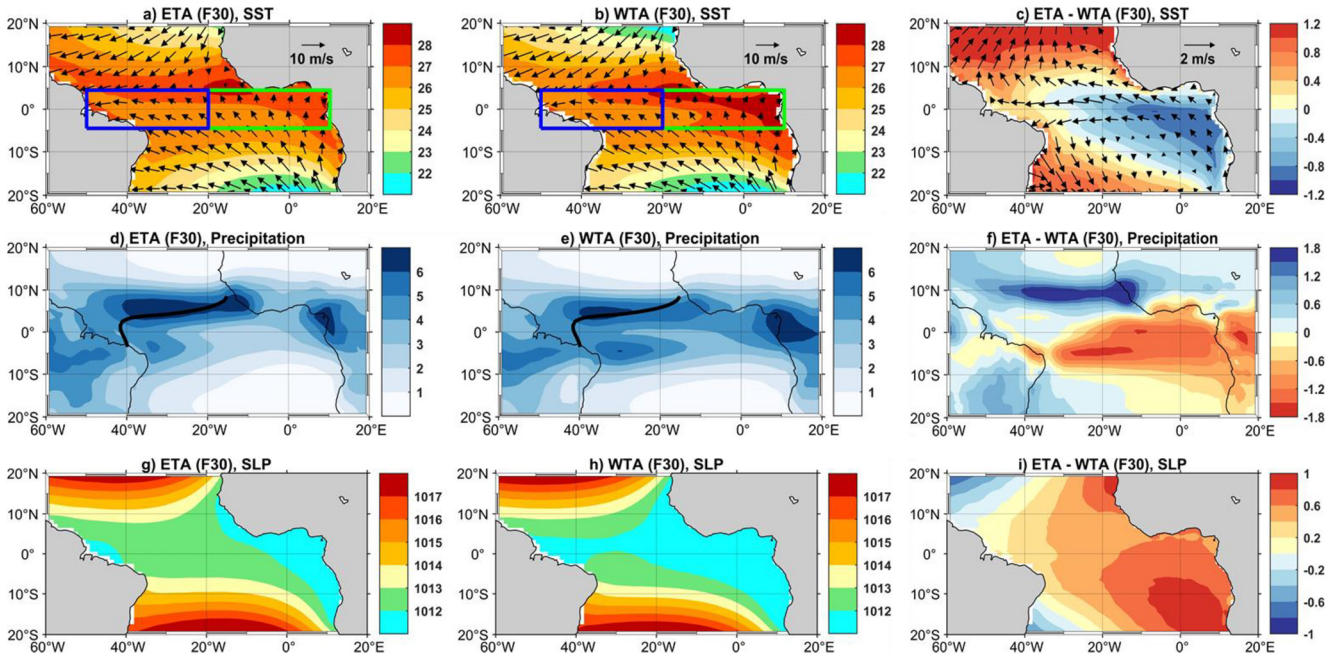

Figure 2. Mean-state sea surface temperature (SST), precipitation and sea level pressure (SLP). (a–c) SST (°C), (d–f) precipitation (mm·day^{-1}) and (g–i) SLP (hPa) in the ETA (left panels) and WTA models (middle panels), averaged over the first 30 years (F30) and all seasons, and the differences (right panels). Models in the ETA sub-ensemble exhibit a warm bias that is smaller than the grand ensemble-mean bias and simulate a reduced carbon dioxide (CO_2)-forced SST gradient. Models in the WTA sub-ensemble exhibit a warm bias that is larger than the grand ensemble-mean bias and simulate an enhanced CO_2-forced SST gradient.

SST in the west and in the east (W–E) (blue and green boxes in Figures 2a and 2b, respectively). A positive (negative) SST gradient is characterized by higher (lower) SST in the west than in the east.

The SST gradient is important with regard to equatorial ocean-atmosphere interactions, specifically the Bjerknes-feedback loop (e.g., Keenlyside & Latif, 2007). The Bjerknes-feedback loop is a positive (amplifying) feedback that involves zonal wind stress anomalies over the western, and thermocline depth and SST anomalies in the eastern equatorial Atlantic. We relate the CO_2-forced trend in the SST gradient to the warm bias (Figure 1a), where the trend is defined as the difference of the trends averaged over the western and eastern equatorial Atlantic. The ensemble-mean CO_2-forced trend in the SST gradient amounts to −0.13°C per 140 years with a range of approximately 1°C (−0.7°C–+0.3°C) per 140 years. There is a statistically significant correlation amounting to 0.60 between the warm bias and the CO_2-forced trend in the SST gradient: models exhibiting a small (large) warm bias tend to simulate a reduced (strengthened) SST gradient. The correlation is 0.73 in CMIP5 and 0.48 in CMIP6, both significant at the 95% confidence level according to the Student's t-test.

The observed SST gradient averaged over 1950–2019, depending on data set, approximately ranges between 0.6°C and 0.8°C (Figure 1b). Most models, however, simulate a negative SST gradient during F30, with an ensemble-mean SST gradient of −0.6°C (Figure 1b), reflecting the models' difficulty to simulate a cold tongue. The correlation between the CO_2-forced trends in the SST gradient and the time-averaged SST gradients simulated during F30 is −0.61, without much difference between CMIP5 (−0.58) and CMIP6 (−0.64). Thus, models exhibiting a large (small) SST gradient during F30 tend to simulate a reduced (stronger) SST gradient in response to elevated atmospheric CO_2-levels. Further, all models that exhibit a positive SST gradient during F30 predict a reduced SST gradient, while all models predicting an enhanced SST gradient exhibit a negative SST gradient during F30 (Figure 1b). Only the former models are consistent with the SST observations during 1950–2019, exhibiting a positive time-averaged SST gradient and negative SST-gradient trend in all analyzed data sets, with the latter ranging between −0.11°C per 70 years and −0.47°C per 70 years (not shown).

The Atlantic Walker Circulation (AWC) is a thermodynamic direct zonal atmospheric circulation cell at the equator, which interacts with the SST gradient as part of the Bjerknes-feedback loop. A box-based index of the Pacific Walker Circulation (PWC) was defined by Vecchi et al. (2006) as the SLP contrast across the equatorial Pacific. Here, an index of the AWC is obtained by calculating the SLP contrast across the equatorial Atlantic (SLP gradient hereafter), using the same boxes as in the definition of the SST gradient, where the SLP gradient is defined by the difference between the eastern and western box (E–W). A negative (positive) change in the SLP gradient implies weaker (stronger) AWC and equatorial trade winds. Models that simulate a reduced CO_2-forced SST gradient also tend to simulate a reduced SLP gradient and vice versa, as illustrated by the correlation of 0.78 (Figure 1c). Again, there is not much difference in the correlation between CMIP5 (0.76) and CMIP6 (0.79). The observations hardly yield any long-term trend in the SLP gradient (not shown). Meng et al. (2012) discuss observational uncertainties and present atmosphere model simulations forced by observed SST 1900–2007 and an estimate of radiative forcing. These uncoupled simulations yield long-term SLP trends over the TA in line with those CMIP models that predict a major reduction of the SST gradient.

Finally, although the SST and precipitation trends do show some seasonal dependences (Figures S2 and S3), the seasonal dependence of the scatter plots shown in Figure 1 is weak, as shown for the cold tongue season June–September (JJAS, Figure S4).

3.2. Sub-Ensembles

We define two sub-ensembles, ETA and WTA. ETA (WTA) models exhibit smaller (larger) warm bias than the ensemble-mean bias and simulate a reduced (enhanced) SST gradient in response to higher atmospheric CO_2-concentrations. There are different aspects that can be considered when defining sub-ensembles such as equal number of models. Since, both warm-bias strength and sign of CO_2-forced SST-gradient change are important with regard to ocean-atmosphere interactions and climate change impacts, we have chosen these two factors. The drawback is that the number of models in WTA (11) is considerably smaller than that in ETA (20). On the other hand, the WTA models can be considered as unrealistic when compared to the SST observations since the mid-20th century, both with respect to the SST climatology and the SST trends. Moreover, it is of interest how the CO_2-forced climate changes in these models differ from that in the ETA models.

Time-averaged fields of selected variables simulated during F30 are calculated for each sub-ensemble (Figure 2). SST differences between ETA (Figure 2a) and WTA models (Figure 2b) exhibit a cold tongue-like pattern (Figure 2c). Further, ETA models simulate stronger southeasterly near-surface (10 m) winds (Figure 2a) than WTA-models (Figure 2b), as exemplified by the wind differences (Figure 2c). Stronger southeasterly winds strengthen coastal and equatorial upwelling, which cools the SST by bringing more cold subsurface waters to the surface. ETA models suffer less from the double-ITCZ problem (e.g., Biasutti et al., 2006; Lin, 2007; Richter & Xie, 2008) than WTA models (Figures 2d and 2e). The former simulate more precipitation north of the equator and less precipitation at and south of the equator than the latter, which is reflected in the marked meridional dipole structure of the differences (Figure 2f). The rainfall differences are dynamically consistent with the near-surface wind differences exhibiting strong cross-equatorial flow (Figure 2c). ETA models (Figure 2g) simulate higher pressure than WTA models (Figure 2h) over large parts of the TA, with largest differences in the southeast (Figure 2i). We note that coupled feedbacks are important in shaping the mean-state in the tropics (Xie, 2009).

3.3. Maps of CO_2-Forced Trends

ETA models (Figure 3a) typically simulate a larger basin-averaged SST warming than WTA models (Figure 3b). One cause could be the different transient climate response (TCR): ETA models exhibit an averaged TCR of 2.2°C (4.9°C) at the time of CO_2-doubling (quadrupling), WTA models of 1.7°C (3.8°C) (Table S4). We note that there is no significant correlation between the TCRs and CO_2-forced SST-gradient changes. Further, ETA models predict an Atlantic Niño-like warming and near-surface wind pattern, with largest warming in the cold tongue and westerlies over the central equatorial Atlantic, whereas WTA models

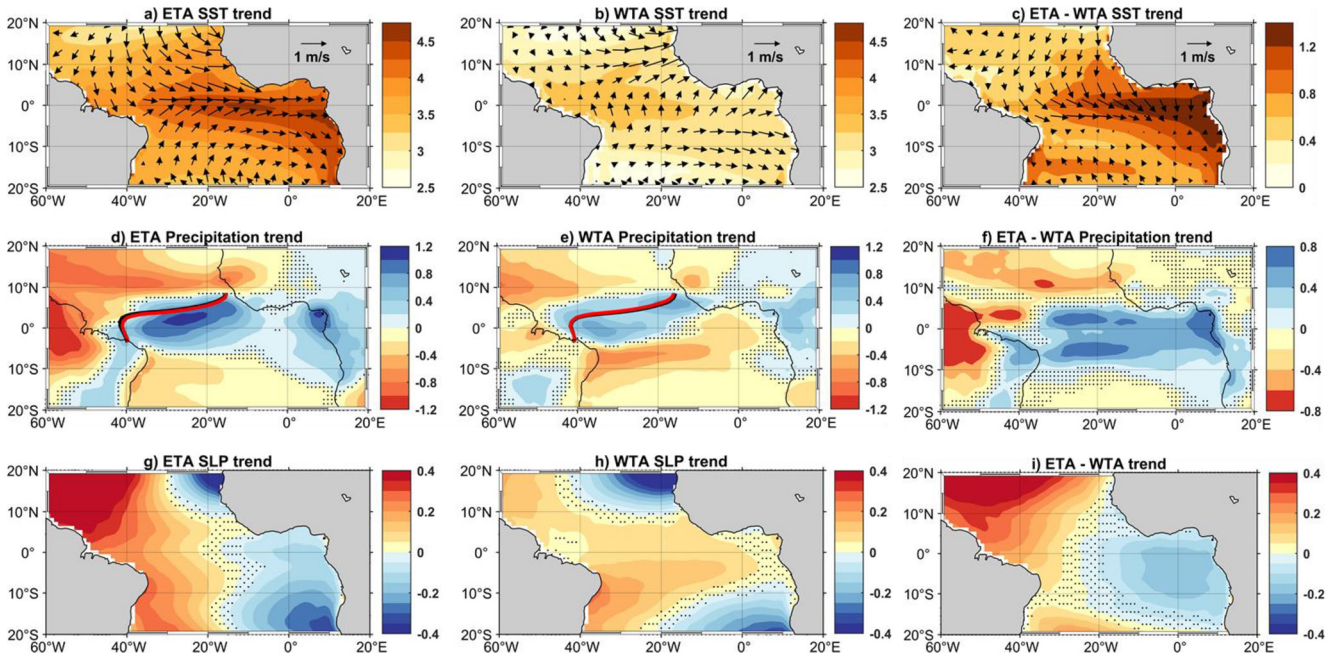

Figure 3. CO_2-forced trends in the two sub-ensembles. CO_2-forced linear trends (per 140 years) of (a–c) sea surface temperature (°C), (d–f) precipitation ($mm \cdot day^{-1}$) and (g–i) sea level pressure (hPa) in the ETA models (left), in the WTA models (middle), and the differences (right). Dots indicate regions where the trend is not significant at the 95% level according to the Spearman's test. In (a–c) the arrows indicate the near-surface (10 m) winds. In (d) and (e) the bold solid lines indicate the position of the ITCZ: the black and red line depict the position during the first and last 30 years of the global warming simulations, respectively. The position of the ITCZ was determined by the zero 10 m meridional wind contour.

simulate a relatively uniform SST warming without strong gradients and relatively weak near-surface wind changes, as exemplified by the corresponding differences (Figure 3c).

ETA models predict enhanced precipitation over the western and central equatorial Atlantic slightly south of the ITCZ, and over western Equatorial Africa (Figure 3d). Over South America and the northern subtropics, they simulate reduced precipitation. While WTA models (Figure 3e) predict a somewhat similar pattern, the changes are much smaller, typically by about 70%. The differences in the precipitation trends are dominated by a zonal dipole in the equatorial region, with reductions over South America and increases over the equatorial Atlantic (Figure 3f), consistent with a zonal reorganization of the AWC, as discussed below (see Figure 5).

The CO_2-forced SLP response too is much larger in the ETA sub-ensemble (Figure 3g) than in the WTA sub-ensemble (Figure 4h). ETA models simulate a dipole-response with falling SLP over the eastern and rising SLP over the western TA, WTA models exhibit a relatively flat pattern. In particular, a reduction of the equatorial SLP gradient, implying AWC slowing and weaker equatorial trade winds, only is observed in the ETA sub-ensemble, as emphasized by the SLP-trend differences (Figure 3i, see also Figure 1c).

3.4. Changes in Atmospheric Circulation

Lindzen and Nigam (1987), considering steady flow and a weak wind regime, relate the divergence of the wind in the boundary layer to the Laplacian of the SST field, a mechanism also referred to as pressure adjustment mechanism (Crespo et al., 2019; Minobe et al., 2008; Nkwinkwa Njouodo et al., 2018). In this mechanism, SST generates a difference of air temperature in the marine atmospheric boundary layer across a front, and the resultant pressure anomalies produce wind convergence (divergence) over warm (cold) water (Shimada & Minobe, 2011). ETA models simulate a marked increase in the SST Laplacian over the equatorial Atlantic (Figure 4a), and also increase in SLP Laplacian (not shown) and near-surface wind convergence (Figure 4d). These changes go along with upward motion (negative values denote upward motion)

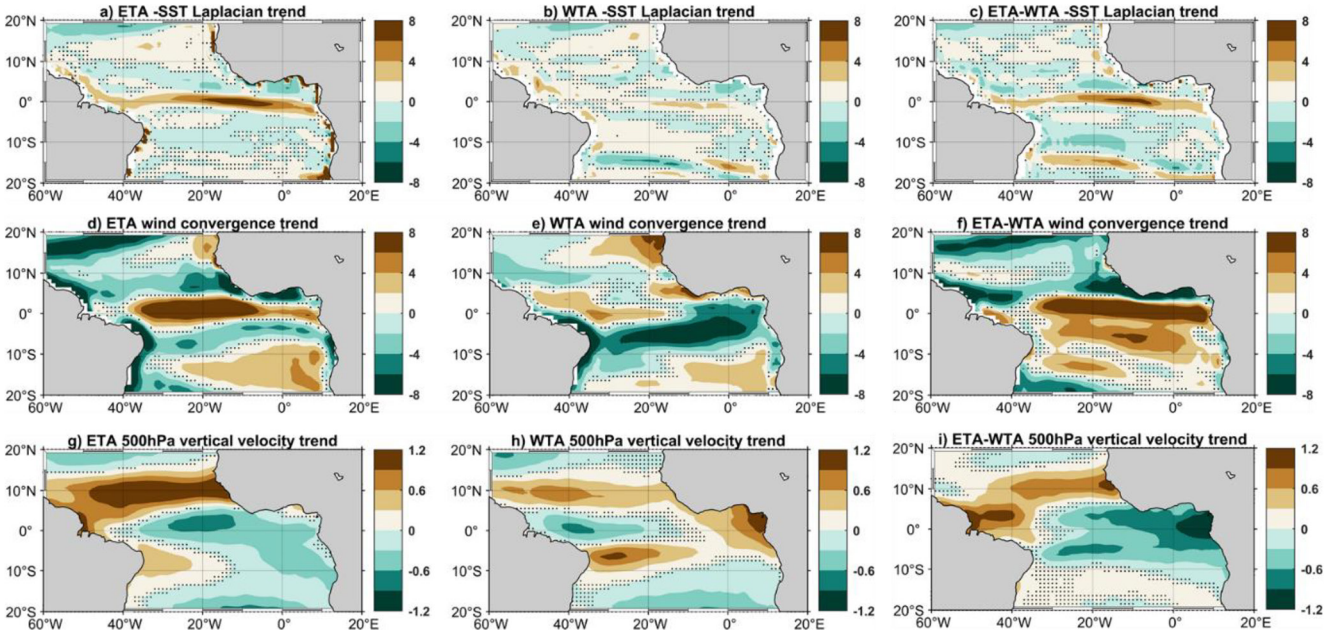

Figure 4. CO_2-forced trends in atmospheric dynamics. CO_2-forced linear trends (per 140 years) of (a–c) sea surface temperature Laplacian (10^{-12}K·m^{-2}), (d–f) near-surface wind convergence (10^{-7}s^{-1}) and (g–i) 500 hPa vertical velocity (Pa·s^{-1}) in the ETA models (left), in the WTA models (middle), and the differences (right). Dots indicate regions where the trend is not significant at the 95% level according to the Spearman's test.

over the cold-tongue region at mid-tropospheric levels that is strongest at the equator near 20°W, and strong subsidence to the north centered around 10°N (Figure 4g).

WTA models simulate small changes in the SST Laplacian (Figure 4b) and near-surface wind convergence at the equator (Figure 4e). An increase in the mid-tropospheric vertical velocity is simulated over the western and a decrease over the far eastern equatorial Atlantic (Figure 4h). There is a band of strong wind divergence, stretching from the western TA at around 10°S to the eastern equatorial TA (Figure 4e), which is associated with subsidence in the mid-troposphere (Figure 4h). Downward motion is particularly strong off the coast of western Equatorial Africa, which is consistent with the lack of significant rainfall response there (Figure 3e). In contrast, ETA models predict significant rainfall increases over this region (Figure 3d).

Finally, we address the AWC by investigating the zonal overturning stream function (Figure 5). ETA models (contours in Figure 5a) exhibit a stronger mean-state (F30) upward branch of the AWC than WTA models (contours in Figure 5b), which is consistent with the stronger easterly trade winds. The AWC strongly changes in the ETA models (color shading in Figure 5a) but not in the WTA models (color shading in Figure 5b). In particular, there is major reorganization of the AWC in the ETA models (Figure 5a), with an eastward extension of its upward branch and a strong weakening of its downward branch over the east.

4. Discussion

This study shows a strong mean-state sensitivity of the TA sector's climate response to increasing atmospheric CO_2-levels in the CMIP models. In particular, models simulating largest SST warming in the eastern equatorial Atlantic typically exhibit a relatively small warm bias, and only these models simulate major changes in atmospheric circulation and in related quantities such as precipitation. On the other hand, models exhibiting a large warm bias tend to predict largest SST warming in the west and much smaller atmospheric changes.

However, the detailed mechanisms underlying the relationship between the mean-state SST and CO_2-forced climate change remain unclear. The models differ in many respects, with regard to physical parameterizations, resolution (horizontal and vertical), and numerical schemes. Atmosphere-model resolution largely explains the relationship between the mean state and the CO_2-forced climate change in the KCM, as

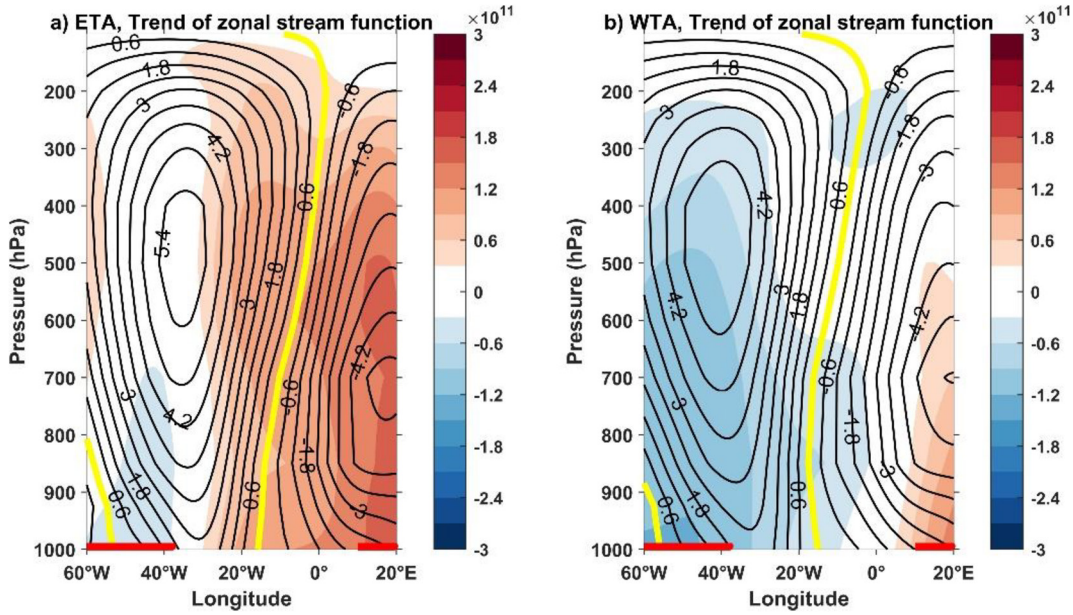

Figure 5. CO_2-forced trends in zonal overturning stream function. Mean state (contours, F30) and trends per 140 years (color) of the zonal overturning stream function ($kg \cdot s^{-1}$) along the equator, averaged from 4.5°N to 4.5°S in the (a) ETA models and (b) WTA models. Yellow contours denote the zero stream function contours. Red bold lines at the bottom represent Africa and South America.

reported by Park and Latif (2020). Their results are consistent with the findings presented here in that only the KCM version exhibiting a small warm bias and realistic SST gradient simulates a reduced SST gradient, that is, more SST warming in the eastern than western TA.

In the CMIP ensemble, the warm bias is not strongly linked to model resolution (Figures S4 and S5). We note that the model labeled "f" in Figure 1 is not considered in the following, because, differently to the other models, flux adjustments are applied, so that the model cannot be used to study resolution effects on the climatology. The zonal atmospheric resolution appears to play some role for the warm bias, exhibiting a correlation with the warm bias of 0.34 when considering all models, which is significant at the 95% confidence level. The correlation in CMIP5 (CMIP6) models amounts to 0.48 (0.25) (Figure S5a). The CMIP6 models typically employ higher zonal resolution in the atmospheric component, but coupled models with an atmospheric resolution higher than 1.5° exhibit still widely varying warm biases. With respect to zonal oceanic resolution, the correlation is 0.21 and not significant at the 95% level. Regarding meridional resolution, correlations with the warm bias amount to 0.22 (atmosphere, Figure S6a) and 0.23 (ocean, Figure S6b), which both are not significant at the 95% level. We note that in the KCM (Park & Latif, 2020), high atmospheric resolution was key to substantially reducing the warm bias.

Tozuka et al. (2011) studied three versions of the same coupled model differing only in the cumulus convection scheme, and one version successfully simulated the SST gradient across the equatorial Atlantic. However, to our knowledge global warming simulations have not been published with the three models. In order to obtain more insight into the processes behind the relationship between mean-state SST and CO_2-forced TA-sector climate change found in the CMIP models, it would be desirable to conduct global warming simulations with models of the same family, which only differ in one or very few aspects.

What is the influence of remote forcing on the TA sector's climate response to increasing CO_2-levels, especially from the tropical Pacific that is known to influence climate variability over the TA region? This question only can be adequately addressed by special global warming experiments in which certain processes are inhibited. Such experiments, however, are not part of CMIP. Park and Latif (2020), by performing uncoupled atmosphere model experiments, find an important role of local processes for determining the KCM's CO_2-forced climate response over the equatorial Atlantic. The CMIP models simulate CO_2-forced changes that are dynamically consistent with this view. For example, the response of the ETA models can

be described as an Atlantic Niño-like response involving reduced zonal SST gradient and weaker equatorial trade winds.

The SSTs in the TA have warmed substantially during the instrumental period and particularly in the southeastern part (Meng et al., 2012; Park & Latif, 2020; Servain et al., 2014; Tokinaga & Xie, 2011). Vizy and Cook (2016) report significant warming trends during 1982–2013 along the Guinean and Angolan/Namibian Coasts, and a cooling trend over the subtropical South Atlantic between 18°S and 28°S. Tokinaga and Xie (2011) report weakening of the equatorial Atlantic cold tongue over the past six decades. Specifically, the eastward-intensified warming leads to enhanced atmospheric convection in the equatorial eastern Atlantic region, as well as to less vigorous trade winds. Meng et al. (2012) describe from observations an eastward-amplified SST warming trend over the TA during the 20th and early 21st century. Only the SST trends simulated by the ETA models are consistent with the aforementioned observations, so that the response of these models may serve as a fingerprint of CO_2-induced climate change in the TA region. We note that there is considerable uncertainty with regard to the SST observations during the last decades (e.g., Vizy & Cook, 2016). Nevertheless, on the basis of this study it appears likely that the distinct spatial structure of the long-term SST warming observed in the TA, exhibiting the largest warming in the east, is related to the rising atmospheric CO_2-levels.

The mean-state dependence of CO_2-forced TA-sector climate change can help to reduce uncertainty in 21st century projections by giving larger weight to those climate models which more realistically simulate TA SST instead of calculating the unweighted average over all models. A weighted ensemble average computed in this way would yield considerably larger and in part qualitatively different changes than the unweighted average and enhance the signal-to-noise ratio, which is important for assessing regional climate changes and related ecological and socioeconomic impacts.

Data Availability Statement

Details on data availability are given in the Supplementary Material. All data used are publicly available on the following websites: CMIP5/6 (https://www.dkrz.de/up/services/data-management/cmip-data-pool), HadiSST (https://www.metoffice.gov.uk/hadobs/hadisst/), ERSSTv5 (https://psl.noaa.gov/data/gridded/data.noaa.ersst.v5.html), COBE-SST2 (https://psl.noaa.gov/data/gridded/data.cobe2.html), NCEP-NCAR (https://rda.ucar.edu/datasets/ds090.2/), HadSLP (https://psl.noaa.gov/data/gridded/data.hadslp2.html), ICOADS (http://www.esrl.noaa.gov/psd/data/gridded/data.coads.2deg.html).

Acknowledgments
The authors thank Dr. Sebastian Steinig for some initial analyses and Dr. Tobias Bayr for helping with the stream function analysis. This work was supported by the RACE project of the German Ministry of Education and Research (BMBF) and by the ROADMAP project funded by JPI Climate and JPI Oceans. Open access funding enabled and organized by Projekt DEAL.

References

Allan, R., & Ansell, T. (2006). A new globally complete monthly historical gridded mean sea level pressure dataset (HadSLP2): 1850–2004. *Journal of Climate*, *19*(22), 5816–5842. https://doi.org/10.1175/jcli3937.1

Biasutti, M., Sobel, A. H., & Kushnir, Y. (2006). AGCM precipitation biases in the tropical Atlantic. *Journal of Climate*, *19*(6), 935–958. https://doi.org/10.1175/jcli3673.1

Cabos, W., Sein, D. V., Pinto, J. G., Fink, A. H., Koldunov, N. V., Alvarez, F., et al. (2017). The South Atlantic Anticyclone as a key player for the representation of the tropical Atlantic climate in coupled climate models. *Climate Dynamics*, *48*(11–12), 4051–4069. https://doi.org/10.1007/s00382-016-3319-9

Crespo, L. R., Keenlyside, N., & Koseki, S. (2019). The role of sea surface temperature in the atmospheric seasonal cycle of the equatorial Atlantic. *Climate Dynamics*, *52*(9), 5927–5946. https://doi.org/10.1007/s00382-018-4489-4

Davey, M., Huddleston, M., Sperber, K., Braconnot, P., Bryan, F., Chen, D., et al. (2002). STOIC: A study of coupled model climatology and variability in tropical ocean regions. *Climate Dynamics*, *18*(5), 403–420.

Deser, C., Lehner, F., Rodgers, K. B., Ault, T., Delworth, T. L., DiNezio, P. N., et al. (2020). Insights from Earth system model initial-condition large ensembles and future prospects. *Nature Climate Change*, *10*, 277–286. https://doi.org/10.1038/s41558-020-0731-2

Eyring, V., Bony, S., Meehl, G. A., Senior, C. A., Stevens, B., Stouffer, R. J., & Taylor, K. E. (2016). Overview of the Coupled Model Intercomparison Project Phase 6 (CMIP6) experimental design and organization. *Geoscientific Model Development*, *9*(5), 1937–1958. https://doi.org/10.5194/gmd-9-1937-2016

Freeman, E., Woodruff, S. D., Worley, S. J., Lubker, S. J., Kent, E. C., Angel, W. E., et al. (2017). ICOADS Release 3.0: A major update to the historical marine climate record. *International Journal of Climatology*, *37*(5), 2211–2232. https://doi.org/10.1002/joc.4775

Harlaß, J., Latif, M., & Park, W. (2018). Alleviating tropical Atlantic sector biases in the Kiel climate model by enhancing horizontal and vertical atmosphere model resolution: Climatology and interannual variability. *Climate Dynamics*, *50*(7), 2605–2635. https://doi.org/10.1007/s00382-017-3760-4

Hawkins, E., & Sutton, R. (2009). The potential to narrow uncertainty in regional climate predictions. *Bulletin of the American Meteorological Society*, *90*(8), 1095–1108. https://doi.org/10.1175/2009bams2607.1

Hersbach, H., Bell, B., Berrisford, P., Horányi, A., Sabater, J. M., Nicolas, J., et al. (2019). Global reanalysis: Goodbye ERA-Interim, hello ERA5. *ECMWF newsletter*, *159*, 17–24.

Hirahara, S., Ishii, M., & Fukuda, Y. (2014). Centennial-scale sea surface temperature analysis and its uncertainty. *Journal of Climate*, *27*(1), 57–75. https://doi.org/10.1175/jcli-d-12-00837.1

Huang, B., Thorne, P. W., Banzon, V. F., Boyer, T., Chepurin, G., Lawrimore, J. H., et al. (2017). Extended reconstructed sea surface temperature, version 5 (ERSSTv5): Upgrades, validations, and intercomparisons. *Journal of Climate*, *30*(20), 8179–8205. https://doi.org/10.1175/jcli-d-16-0836.1

IPCC. (2014). Climate Change 2014: Synthesis Report. In Core Writing Team, R. K. Pachauri, and L. A. Meyer (Eds.), Contribution of Working Groups I, II and III to the Fifth Assessment Report of the Intergovernmental Panel on Climate Change. IPCC, Geneva, Switzerland, p. 151.

Kalnay, E., Kanamitsu, M., Kistler, R., Collins, W., Deaven, D., Gandin, L., et al. (1996). The NCEP/NCAR 40-year reanalysis project. *Bulletin of the American Meteorological Society*, *77*(3), 437–471. https://doi.org/10.1175/1520-0477(1996)077<0437:tnyrp>2.0.co;2

Kay, J. E., Deser, C., Phillips, A., Mai, A., Hannay, C., Strand, G., et al. (2015). The Community Earth System Model (CESM) large ensemble project: A community resource for studying climate change in the presence of internal climate variability. *Bulletin of the American Meteorological Society*, *96*(8), 1333–1349. https://doi.org/10.1175/bams-d-13-00255.1

Keenlyside, N. S., & Latif, M. (2007). Understanding equatorial Atlantic interannual variability. *Journal of Climate*, *20*(1), 131–142. https://doi.org/10.1175/jcli3992.1

Lin, J. L. (2007). The double-ITCZ problem in IPCC AR4 coupled GCMs: Ocean–atmosphere feedback analysis. *Journal of Climate*, *20*(18), 4497–4525. https://doi.org/10.1175/jcli4272.1

Lindzen, R. S., & Nigam, S. (1987). On the role of sea surface temperature gradients in forcing low-level winds and convergence in the tropics. *Journal of the Atmospheric Sciences*, *44*(17), 2418–2436. https://doi.org/10.1175/1520-0469(1987)044<2418:otross>2.0.co;2

Meng, Q., Latif, M., Park, W., Keenlyside, N. S., Semenov, V. A., & Martin, T. (2012). Twentieth century Walker circulation change: Data analysis and model experiments. *Climate Dynamics*, *38*(9–10), 1757–1773. https://doi.org/10.1007/s00382-011-1047-8

Meynadier, R., de Coëtlogon, G., Leduc-Leballeur, M., Eymard, L., & Janicot, S. (2016). Seasonal influence of the sea surface temperature on the low atmospheric circulation and precipitation in the eastern equatorial Atlantic. *Climate Dynamics*, *47*(3), 1127–1142. https://doi.org/10.1007/s00382-015-2892-7

Milinski, S., Bader, J., Haak, H., Siongco, A. C., & Jungclaus, J. H. (2016). High atmospheric horizontal resolution eliminates the wind-driven coastal warm bias in the southeastern tropical Atlantic. *Geophysical Research Letters*, *43*(19), 10–455. https://doi.org/10.1002/2016gl070530

Minobe, S., Kuwano-Yoshida, A., Komori, N., Xie, S. P., & Small, R. J. (2008). Influence of the Gulf Stream on the troposphere. *Nature*, *452*(7184), 206–209. https://doi.org/10.1038/nature06690

Nkwinkwa Njouodo, A. S., Koseki, S., Keenlyside, N., & Rouault, M. (2018). Atmospheric signature of the Agulhas Current. *Geophysical Research Letters*, *45*(10), 5185–5193. https://doi.org/10.1029/2018gl077042

Park, W., & Latif, M. (2020). Resolution dependence of CO2-induced Tropical Atlantic sector climate changes. *npj Climate and Atmospheric Science*, *3*(1), 1–8. https://doi.org/10.1038/s41612-020-00139-6

Rayner, N. A. A., Parker, D. E., Horton, E. B., Folland, C. K., Alexander, L. V., Rowell, D. P., et al. (2003). Global analyses of sea surface temperature, sea ice, and night marine air temperature since the late nineteenth century. *Journal of Geophysical Research*, *108*(D14), 4407. https://doi.org/10.1029/2002jd002670

Richter, I., & Tokinaga, H. (2020). An overview of the performance of CMIP6 models in the tropical Atlantic: Mean state, variability, and remote impacts. *Climate Dynamics*, *55*(9), 2579–2601. https://doi.org/10.1007/s00382-020-05409-w

Richter, I., & Xie, S. P. (2008). On the origin of equatorial Atlantic biases in coupled general circulation models. *Climate Dynamics*, *31*(5), 587–598. https://doi.org/10.1007/s00382-008-0364-z

Richter, I., Xie, S. P., Behera, S. K., Doi, T., & Masumoto, Y. (2014). Equatorial Atlantic variability and its relation to mean state biases in CMIP5. *Climate Dynamics*, *42*(1–2), 171–188. https://doi.org/10.1007/s00382-012-1624-5

Servain, J., Caniaux, G., Kouadio, Y. K., McPhaden, M. J., & Araujo, M. (2014). Recent climatic trends in the tropical Atlantic. *Climate Dynamics*, *43*(11), 3071–3089. https://doi.org/10.1007/s00382-014-2168-7

Shepherd, T. G. (2014). Atmospheric circulation as a source of uncertainty in climate change projections. *Nature Geoscience*, *7*(10), 703–708. https://doi.org/10.1038/ngeo2253

Shimada, T., & Minobe, S. (2011). Global analysis of the pressure adjustment mechanism over sea surface temperature fronts using AIRS/Aqua data. *Geophysical Research Letters*, *38*, L06704. https://doi.org/10.1029/2010GL046625

Siongco, A. C., Hohenegger, C., & Stevens, B. (2015). The Atlantic ITCZ bias in CMIP5 models. *Climate Dynamics*, *45*(5–6), 1169–1180. https://doi.org/10.1007/s00382-014-2366-3

Steinig, S., Harlaß, J., Park, W., & Latif, M. (2018). Sahel rainfall strength and onset improvements due to more realistic Atlantic cold tongue development in a climate model. *Scientific Reports*, *8*, 2569. https://doi.org/10.1038/s41598-018-20904-1

Taylor, K. E., Stouffer, R. J., & Meehl, G. A. (2012). An overview of CMIP5 and the experiment design. *Bulletin of the American Meteorological Society*, *93*(4), 485–498. https://doi.org/10.1175/bams-d-11-00094.1

Tokinaga, H., & Xie, S. P. (2011). Weakening of the equatorial Atlantic cold tongue over the past six decades. *Nature Geoscience*, *4*(4), 222–226. https://doi.org/10.1038/ngeo1078

Tozuka, T., Doi, T., Miyasaka, T., Keenlyside, N., & Yamagata, T. (2011). Key factors in simulating the equatorial Atlantic zonal sea surface temperature gradient in a coupled general circulation model. *Journal of Geophysical Research*, *116*, C06010. https://doi.org/10.1029/2010JC006717

Vecchi, G. A., Soden, B. J., Wittenberg, A. T., Held, I. M., Leetmaa, A., & Harrison, M. J. (2006). Weakening of tropical Pacific atmospheric circulation due to anthropogenic forcing. *Nature*, *441*(7089), 73–76. https://doi.org/10.1038/nature04744

Vizy, E. K., & Cook, K. H. (2016). Understanding long-term (1982–2013) multi-decadal change in the equatorial and subtropical South Atlantic climate. *Climate Dynamics*, *46*, 2087–2113. https://doi.org/10.1007/s00382-015-2691-1

Wengel, C., Latif, M., Park, W., Harlaß, J., & Bayr, T. (2018). Seasonal ENSO phase locking in the Kiel Climate Model: The importance of the equatorial cold sea surface temperature bias. *Climate Dynamics*, *50*, 901–919. https://doi.org/10.1007/s00382-017-3648-3

Willeit, M., Ganopolski, A., Calov, R., & Brovkin, V. (2019). Mid-Pleistocene transition in glacial cycles explained by declining CO_2 and regolith removal. *Science Advances*, *5*(4), eaav7337. https://doi.org/10.1126/sciadv.aav7337

Wills, R. C., Battisti, D. S., Armour, K. C., Schneider, T., & Deser, C. (2020). Pattern recognition methods to separate forced responses from internal variability in climate model ensembles and observations. *Journal of Climate*, *33*(20), 8693–8719. https://doi.org/10.1175/jcli-d-19-0855.1

Xie, S. P. (2009). Ocean–atmosphere interaction and tropical climate. In *The encyclopedia of life support systems*. (EOLSS).

Xu, Z., Chang, P., Richter, I., Tang, G., & Tang, G. (2014). Diagnosing southeast tropical Atlantic SST and ocean circulation biases in the CMIP5 ensemble. *Climate Dynamics*, *43*(11), 3123–3145. https://doi.org/10.1007/s00382-014-2247-9

Zuidema, P., Chang, P., Medeiros, B., Kirtman, B. P., Mechoso, R., Schneider, E. K., et al. (2016). Challenges and prospects for reducing coupled climate model SST biases in the eastern tropical Atlantic and Pacific Oceans: The US CLIVAR Eastern Tropical Oceans Synthesis Working Group. *Bulletin of the American Meteorological Society*, *97*(12), 2305–2328. https://doi.org/10.1175/bams-d-15-00274.1